Combined Structural Analysis of Core and Image Log of TGH 76-31 South East of Mt Baker, Washington State

Breeann Stowe¹, Drew Spake², Trenton T. Cladouhos³, and Alex N. Steely⁴, and Nicholas Davatzes¹

¹Temple University, Philadelphia, PA 19122 ²Ormat, Reno, Nevada ³Cyrq Energy, Inc., Seattle, WA

⁴Washington State Department of Natural Resources, Olympia, WA

Keywords

Play Fairway, Image Log, Core, Fracture, Cascades

ABSTRACT

Despite active volcanism, few geothermal energy resources have been developed in the Cascades Range. Temperature Gradient Hole 76-31 was drilled to ~440 m measured depth to probe for zones where fractures provide fluid conduits that transport deep volcanic heat to shallow depths that could support baseload, carbon neutral electrical generation. These zones were predicted by a Play Fairway assessment (PFA) of resource potential along a zone 11 km west-southwest of the summit of Mount Baker Volcano. Rock core, temperature logs, and an acoustic image log were obtained. By comparison to outcrops, the core has been initially interpreted as the Chilliwack group comprised of partially metamorphosed basaltic to andesitic volcanics. Core mapping reveals complex, steeply dipping networks of fractures and brecciation along slickensided strike slip faults; clay alteration is common in many of these structures. The majority of fractures are thoroughly healed by layers of chlorite and calcite; preservation of pyrite indicates anoxic conditions. The majority of fracture porosity resides in very dense fractures a few centimeters or less in length. The image log provides good insights into attitude of fractures that fully transect the core, but generally underestimates fracture density. The combination of complex, non-planar fracture zones containing many short fractures and healing promote misinterpretation of natural fracture attitude and density in the image log. The healing and anoxic minerals are consistent with the conductive temperature gradient measured in the well below a shallow isothermal zone, although, several fractures are open or only partially healed and resulted in fluid entries into the well. The equilibrated measured temperature gradient of 64°C/km and calculated heat flow of 145 mW/m2 is more than twice the regional average, indicating local influence of the Mt Baker magmatic system at the Little Park Creek TGH site.

1. Introduction

Geothermal exploration suffers from several critical limitations. First, geothermal systems are complex and flow tends to be channeled through relatively small volumes sometimes dominated by a discrete fracture network. Second, early data limitations and geological heterogeneity necessarily increase uncertainty in model predictions. Third, drilling to test exploration models is hampered by a combination of difficulty due to inexperience with new sites and challenging drilling conditions if the expected cracking or hydrothermal alteration is present. Cost over-runs are common in this phase due to drilling delays and can cause projects to fail. Finally, once drilled, understanding the conditions encountered along the well, how they test the exploration model, and how they can update it to guide subsequent exploration is difficult and time consuming.

At Mount Baker, temperature gradient hole (TGH) MB76-31 has been drilled to assess the potential for a hydrothermal resource predicted by play fairway modeling (Figure 1a) (Forson et al., 2017). To address the drilling issue, a local drilling company was employed to drill a corehole. The coring process enhanced the value of information from this early well including providing the potential for detailed rock and fracture characterization. It was also found that under the anticipated drilling conditions (weathered rock interspersed with boulders, high pressure water entries, and highly fractured intervals), the coring system improved borehole stability, fluid management, and drilling progress.

Once drilled, repeat temperature surveys provide a direct assessment of resource potential, including a detailed assessment of rock properties such thermal properties for calculating heat flow (Cladouhos et al., 2020), the association of structures with temperature anomalies or water entries, and the population of fractures. Particularly relevant is the history of fracturing and paragenetic alteration that influence the amount and nature of porosity needed to host hydrothermal flow and a reservoir of hot fluid. At shallower depth, core may reveal the assemblage of alteration indicating a hydrothermal cap rock hiding an underlying resource. Alternatively, borehole televiewer (BHTV) logs provide an efficient means of sampling the fracture population, and potentially constraining the stress state if borehole wall failure is detected.

In this contribution, we provide a characterization of the conditions recorded in core and how they inform the PFA model. We further compare these results to an independent analysis of the image log of the well. This has several benefits including: (1) orienting the core; (2) establishing the difference in sampling between the two methods; (3) assessing the relative time-cost of the two approaches.

1.1 PFA

The Play Fairway Analysis (PFA) predicts the presence of hydrothermal circulation. In order for a geothermal system to be suitable as an energy resource, five key elements are required (Figure 1b): (1) a high temperature from a heat source, (2) a structure or mechanism that allows heat to move to shallow depths that are economically accessible by drilling, (3) a volume of highly connected porosity, (4) saturation with water allowing heat to be moved to a power plant (or distribution pumping station) at the surface via pumping, and (5) a location near infrastructure and developable land that allows the energy to be used (Forson et al., 2017).

Maps of heat, permeability, saturation, and combined potential are constructed for areas of interest to pinpoint locations with high potential for hydrothermal circulation (Figure 2). The Washington State Geothermal Play Fairway Analysis (GPFA) constructed a map of heat potential (Figure 2a), for the state of Washington, using limited temperature profiles and bottomhole temperatures in wells, measured temperatures of springs, geothermometry of fluid samples from springs and wells, and maps of Quaternary volcanic vents and intrusive rocks (Forson et al., 2017). Arguing that permeability would most likely be due to dense, connected, and critically stressed fractures, the Washington State GPFA constructed a model of permeability potential (Figure 2b) from fault density, seismic-event density, a model of the current tectonic displacement field from local Global Positioning System (GPS) monitoring, and mechanical modeling of slip and associated elastic distortions along faults (Forson et al., 2015; Swyer et al., 2018). Magnetotelluric (MT) resistivity and seismic-event density were used to infer the potential for fluid-filled fractures (Figure 2c) (Forson et al., 2017). When mapped through a linear weighting scheme, where weights were derived from expert opinion using an analytical hierarchy process (AHP) (Saaty, 2008), heat, permeability, and fluid-filled fracture potential resulted in an estimated combined resource potential for depths of 200 m and 2 km (Figure 2d) (see discussion in Forson et al., 2015, Forson et al., 2016, Forson et al., 2017). Note that not all sites have the same quality of data; for instance, seismic event density was insufficient at Mount Baker to inform the permeability potential criteria. These differences are represented in related uncertainty and development risk assessments (please refer to Forson et al., 2017 for details). Economic feasibility and risk for development were further refined, based on the uncertainty maps, a map of critical infrastructure, and sites available for development (Forson et al., 2016; Forson et al., 2017).

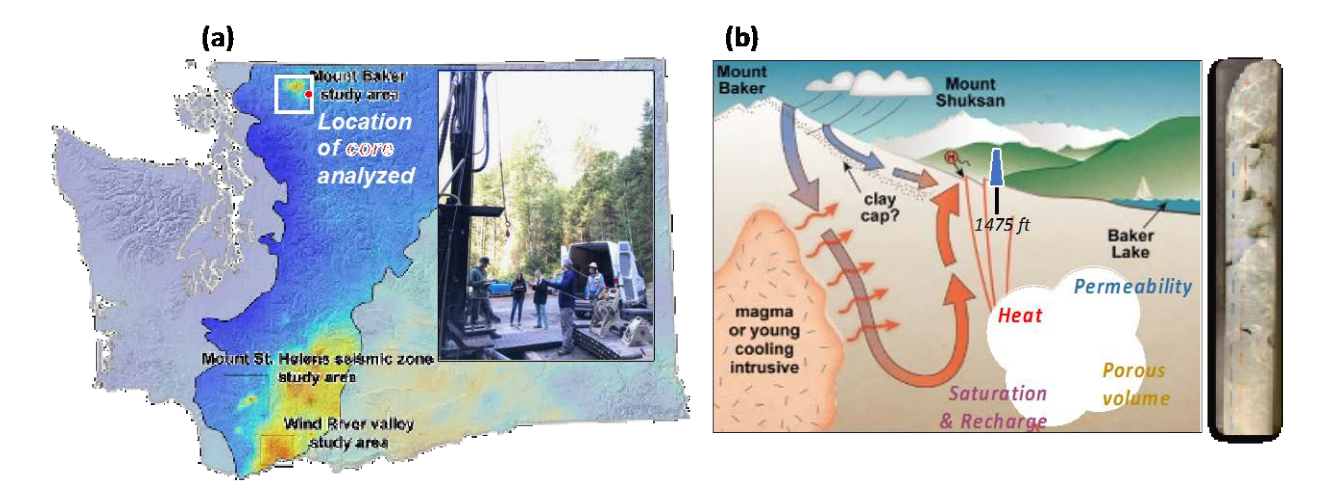


Figure 1: (a) Geothermal resource favorability assessment of the Cascades Range (modified from Boschmann et al., 2014); inset, BHTV logging of the well. (b) Conceptual model for the geothermal resource near Mount Baker (modified from Forson et al., 2017).

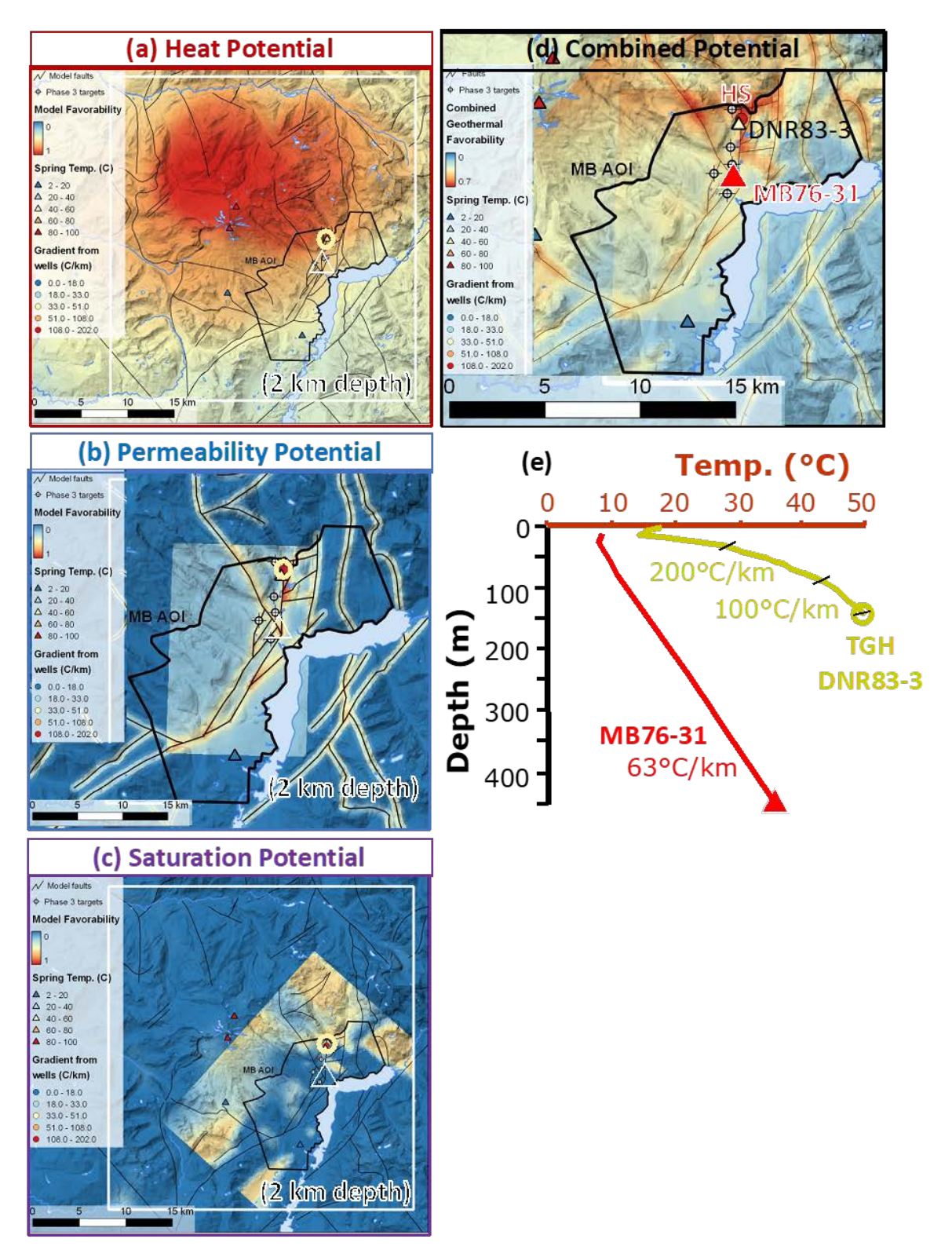


Figure 2: Results of play-fairway analysis, PFA (Forson et al., 2017) including (a) heat potential, (b) permeability potential, (c) saturation potential, and (d) resulting combined potential. Not shown are related assessments of confidence and access used to determine development risk. (e) Equilibrated temperature profile measured in TGH's MB76-31 (Cladouhos et al., 2020) and DNR83-3.

To test the PFA prediction of a geothermal resource (and by extension the methodology), a site was chosen to drill a temperature gradient hole (TGH) where (a) there was a high resource potential, (b) uncertainty in the prediction was moderate to low, and (c) infrastructure and leasing would allow drilling. In 2019, TGH MB 76-31 was drilled by the Washington State GPFA, on the south-eastern flank of Mount Baker (adjacent to the proposed large strike slip fault) to test for the essential components of an active hydrothermal system: (1) heat evident from temperature profiling, (2) saturation and flow in the TGH, and (3) connected porosity and permeability from fractures evident in core and image logs (Figure 1b, 2). Thus, TGH MB76-31 probes for system components where analysis predicts high favorability combined with lease access and infrastructure. Given a shallow depth of 448.5 m, this test is limited to potential cap rock or shallow indicators in the Chilliwack group rather than the reservoir itself.

2. Geological Setting

2.1 Geology and Tectonics

Mount Baker is a multi-vent, andesitic stratovolcano located in the northern Cascade Range of Washington State, USA (Figure 1a, 3). Remaining recurrently active over the past 1.2 million years, its most recent activity lies in the Sherman Craters, exhibiting active steam vents (Crider et al., 2011). Over the past 140 ka, it has erupted andesitic flows with much of its current cone being built since 40ka and the bulk of its uppermost cone since 20 ka (Hildreth et al., 2003; Crider et al., 2011).

The volcano intrudes and overlies the pre-tertiary Bell pass mélange, Permian to Devonian metasedimentary and metavolcanic rocks of the Chilliwack Group, and the middle Jurassic to early Cretaceous marine metasedimentary and metavolcanic rocks of the Cultus Formation and Nooksack Formation (Tabor et al., 2003; Dragovich et al., 2002). The Chilliwack Group is more likely to appear as partially metamorphosed basaltic to andesitic volcanics, sandstone, siltstone, and shale, with limestone occasionally alterated to marble; the Nooksack Formation is more likely to be metamorphosed marine clastics, interfingering or associated with metamorphosed rocks of various grades and compositions. Because the units are composed of very similar lithologies, they are particularly difficult to distinguish in drill cuttings or core. Beyond the local deformation and alteration from volcanic events, the northwestern Cascade Range exhibits regional metamorphism as blue and green schist facies due to the subduction of the Juan de Fuca plate under the North American Plate just off shore. In general, high rainfall and dense vegetation in the region limit outcrop exposure, leading to incomplete characterization of lithologic units and associated geological structures.

However, several large faults have been recognized in and around the study area on the east flank of Mount Baker from lineaments in Light Detection and Ranging (LiDAR), aerial imagery, Digital Elevation Model (DEM), limited seismicity, and surface deformation calculated from gradients in GPS velocities, (Forson et al., 2017) and modeling of ground magnetic data (Witter et al., 2017). Much of the surface deformation can be explained by the deflation of a volcanic chamber 5.8 km deep beneath Mount Baker volcano, that has been modeled as an elastic point source (Hodge and Crider, 2010; Swyer et al., 2018). When compared to other volcanoes in the

Cascade Range of Washington State, such as Mount Rainier or Mount Saint Helens, Mount Baker's seismicity rate is very low (Swyer et al., 2018).

2.2 PFA Model

Despite andesitic flows as young as 6700 years old and magmatic injection detected as recently as 1975-76, surface manifestation of a hydrothermal system is sparse with one hot spring (Baker Hot Springs, Figure 2, 3) and few magmatic gas fumaroles evident in Baker Lake, suggesting reservoir temperatures may reach 150-170°C (Crider et al., 2011; Boschmann et al., 2014; Forson et al., 2017). Two sub-surface geothermal resource types have been proposed that would provide heat and support circulation to the hot spring (Forson et al., 2017):

- (1) A magmatic heat source is at a great depth that may be connected to the near surface faults, acting as conduits, allowing deep convective circulation between the magma body and the surface. In this system, the stored fluid and heat accessible for energy development is hosted in a fault zone.
- (2) A magmatic heat source is intruded at a shallower depth with dikes and sills heating water locally. In this system, the reservoir is constituted by a system of fractures adjacent to the intrusive bodies of magma.

These resource types have been further hypothesized to interact with the Baker Hot Spring, with the most recent model predicting a magma or young cooling intrusive body lying under Mount Baker, largely confined at depth by a well-developed caprock primarily comprised of smectite clays in volcanic metasediments (Crider et al., 2011; Forson et al., 2017). Both models rely on vertically extensive faults with associated high densities of open fractures to connect the deeper heat source to a shallow reservoir viable for geothermal development. And only where faulting breaks through the caprock (or the caprock is incompletely formed) is heat convectively transported to the near surface to feed the hot spring and Baker Lake fumaroles. The candidate fault system is a series of near vertical faults near Baker Lake; the nearby presence of Baker Hot Spring and warm sulfur gas spots in Baker Lake support the potential for modern hydrothermal fluid flow.

3. Methods

TGH MB 76-31 extends to 448.5 m (1471.5 ft) measured depth. Drilling at MB 76-31 began on May 29, 2019; the final day of drilling was August 29, 2019, and the hole was completed with liner installation on September 3, 2019. Bedrock was encountered at 123 ft (37.4 m) below ground surface (BGS) after drilling through a mixture of unconsolidated sand, gravel and clay. From 123 ft (37.4 m) to total depth (TD) at 1471.5 ft (448.5 m) the bedrock lithology is composed of altered volcanic deposits likely representing the Permian, Carboniferous, and Devonian Volcanic Rocks of the Chilliwack Group (PDcv) (Tabor et al., 2003). Temperature logs were gathered repeatedly during drilling with the final log obtained on November 11, 2019 displaying the equilibrium temperature gradient of 63°C/km (Figure 2e) (Cladouhos et al., 2020); less than the ~100°C/km in DNR83-3 (140 m deep) leading to reservoir temperatures estimated at 150-170°C/km from geothermometry (Korosec, 1984) near baker Hot Springs, but more than twice the regional average of ~30°C/km (Blackwell et al., 1990; Boschmann et al., 2014; Cladouhos, 2020).

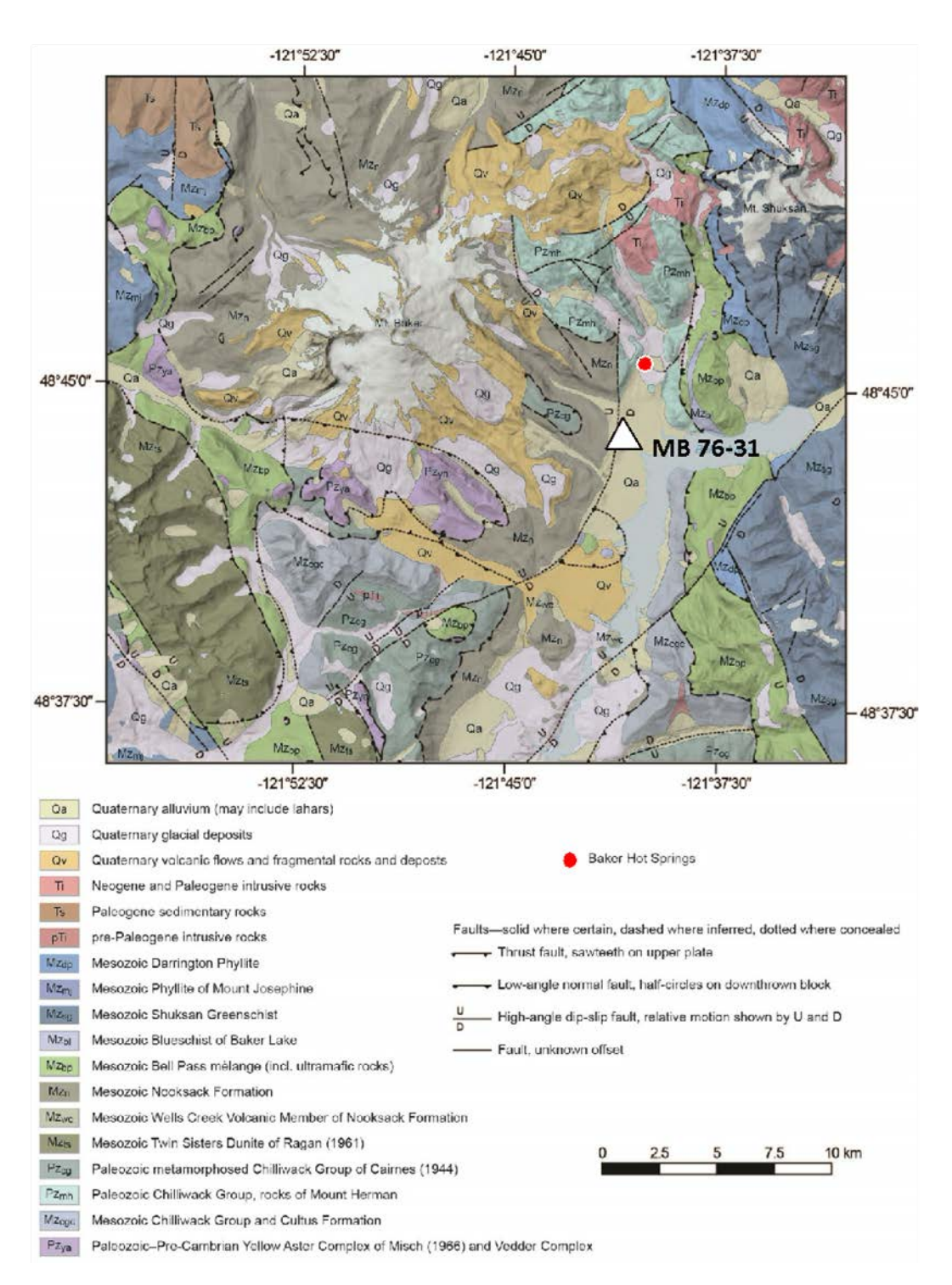


Figure 3: Geological map adapted from Tabor et al., 2003 and Forson et al., 2017).

3.1 Core Mapping

Core is available from a depth of 37.5 m to 417.9 m (123 ft to 1471 ft). Mapping is on-going with priority given to the base of the TGH. To date, boxes 21 (401.4 - 405.5 m; 1317 - 1330.5 ft) and 22 (405.5 - 410.1 m; 1330.5 - 1345.5 ft) have been mapped. These maps are correlated with the BHTV log to independently establish their position and orientation in the TGH.

Maps are initially drawn on acetate overlays after the core is assembled into continuous sections with consistent internal orientation (Figure 4). Highly fragmented sections that are unable to be assembled are not be mapped; the interval is noted as a fragmentation zone for later correlation with the BHTV image. Features greater than 0.05 m in length and 0.002 m in thickness are traced onto the acetate paper overlain on the core. These features include open space, precipitant filling, lithologic units, alteration zones, and breccia zones. Upon completion, the acetate map is unrolled and scanned as a 300 ppi an image file using a drum scanner. Map features are then assigned uniform index colors in photoshop, then the image is cropped and rotated so the y-axis aligns with the up-direction of the TGH, and scaled to a 1:1 ratio.

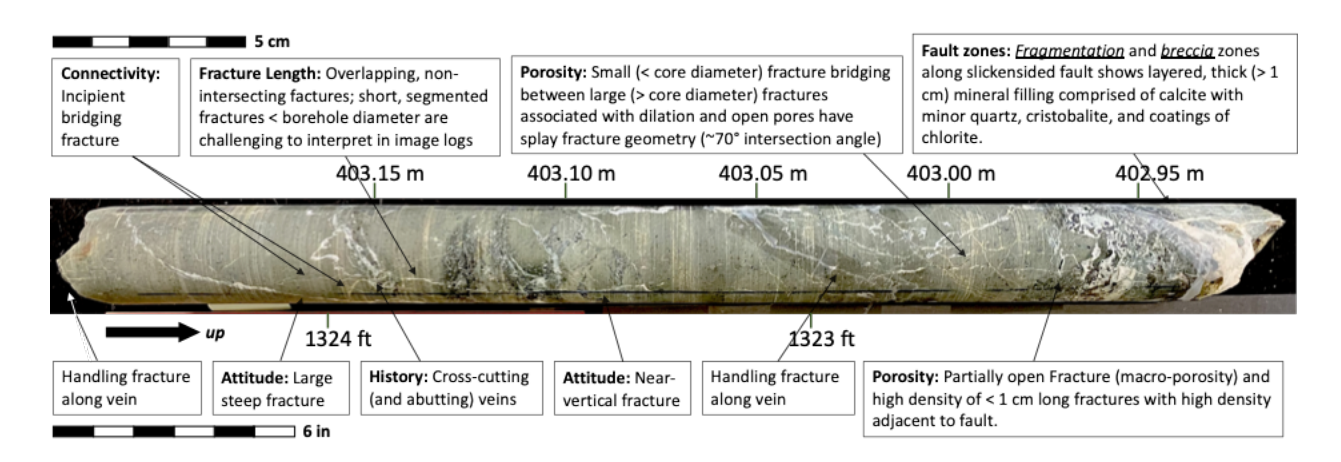


Figure 4: Example structures mapped in the MB76-31 HQ core with diameter of 63.5 mm (2.5 inches) from 1322 to 1324.4 GL.

This digital map is imported into WellCAD in a new data channel where the image is flipped about a vertical axis to match the outward looking direction of the image log, then translated and rotated to correlate unique features present in both the BHTV image (Section 3.2 below) and core map from an initial position based on the measured depth of the core (Figures 6 resulting in Figures 7 and 8). WellCAD is then used to manually fit sinewaves to the mapped features, generating information on the position, attitude, thickness and type of structures along the core, which is the typical approach to image log interpretation as discussed below. Note that the external dimension of the core is smaller than the internal dimension of the TGH, thus the amplitude of sinewave in the core map is proportionately smaller than in the image log; this is accounted for both during correlation and dip calculation.

Core mapping takes ~5 hours to map and digitize each 3 ft (1 m) section of core at a 2 mm scale (excluding compositional or thin section analysis).

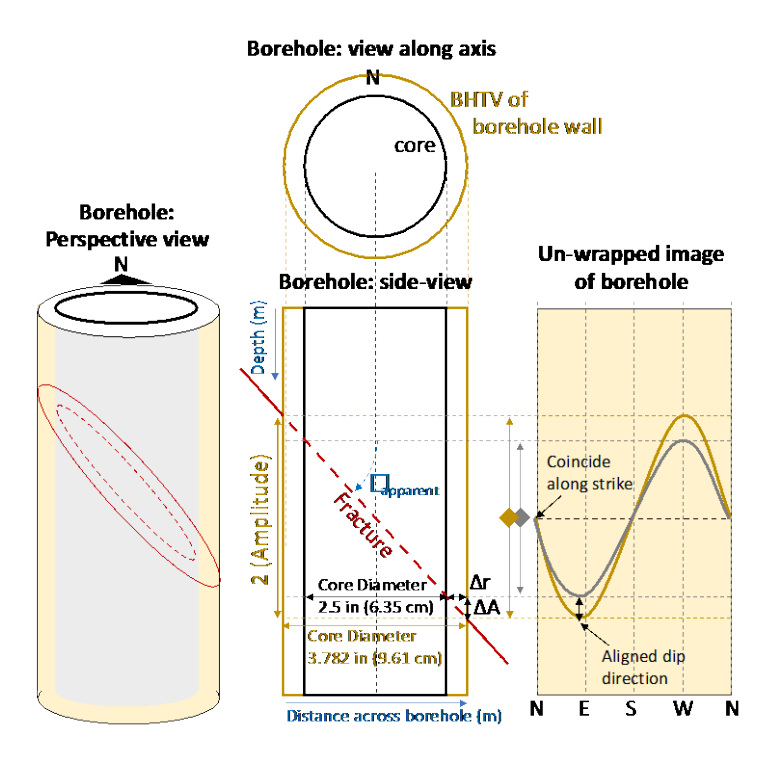


Figure 5: Correlation of fractures in BHTV and in Core.

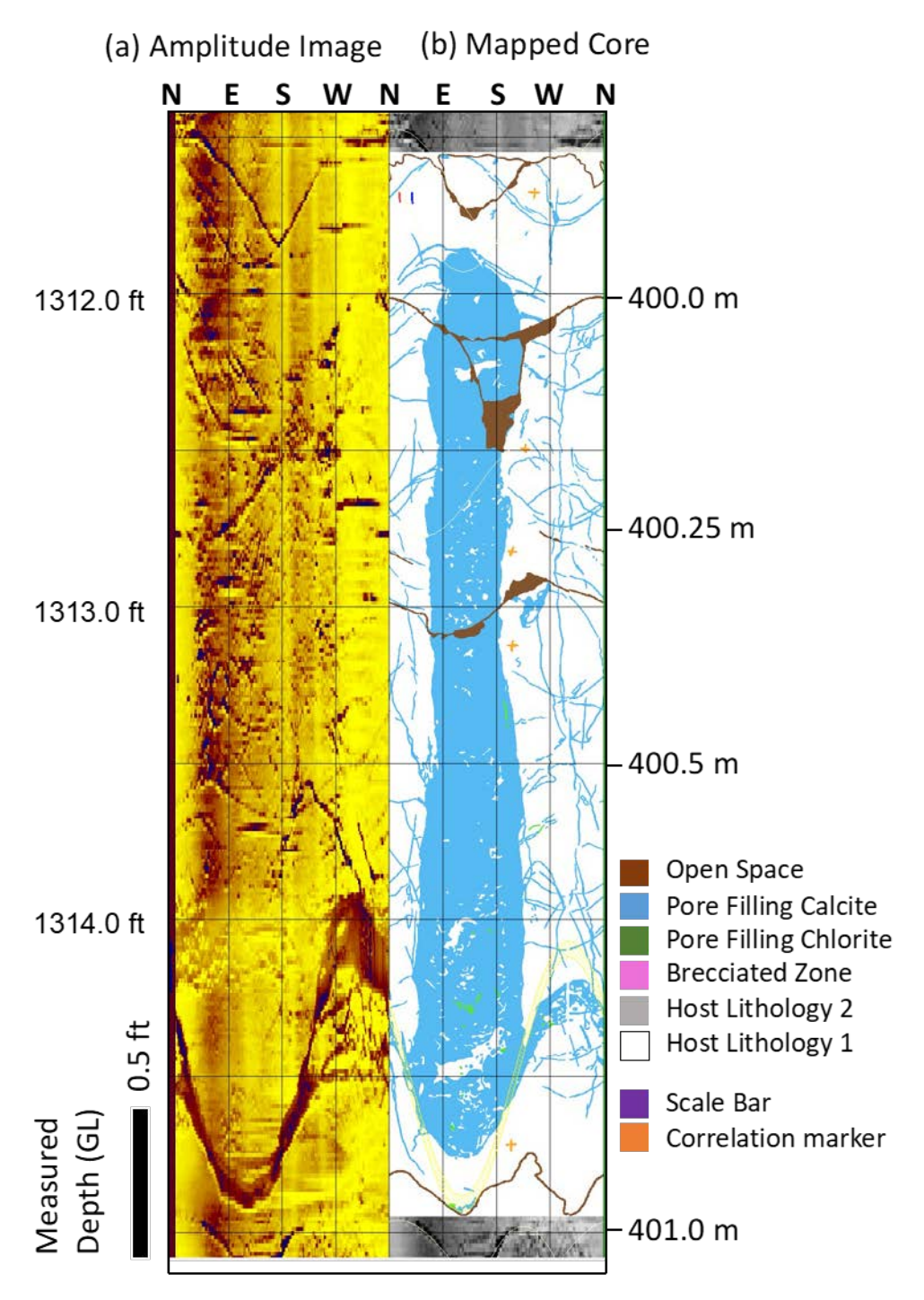


Figure 6: Fractures in BHTV and core after vertical axis reflection and alignment of the core map with the image log. Note that the amplitude of structures in the map is smaller than the corresponding amplitude in the amplitude image proportional to the difference in the outer dimension of the core and the inner dimension of the TGH.

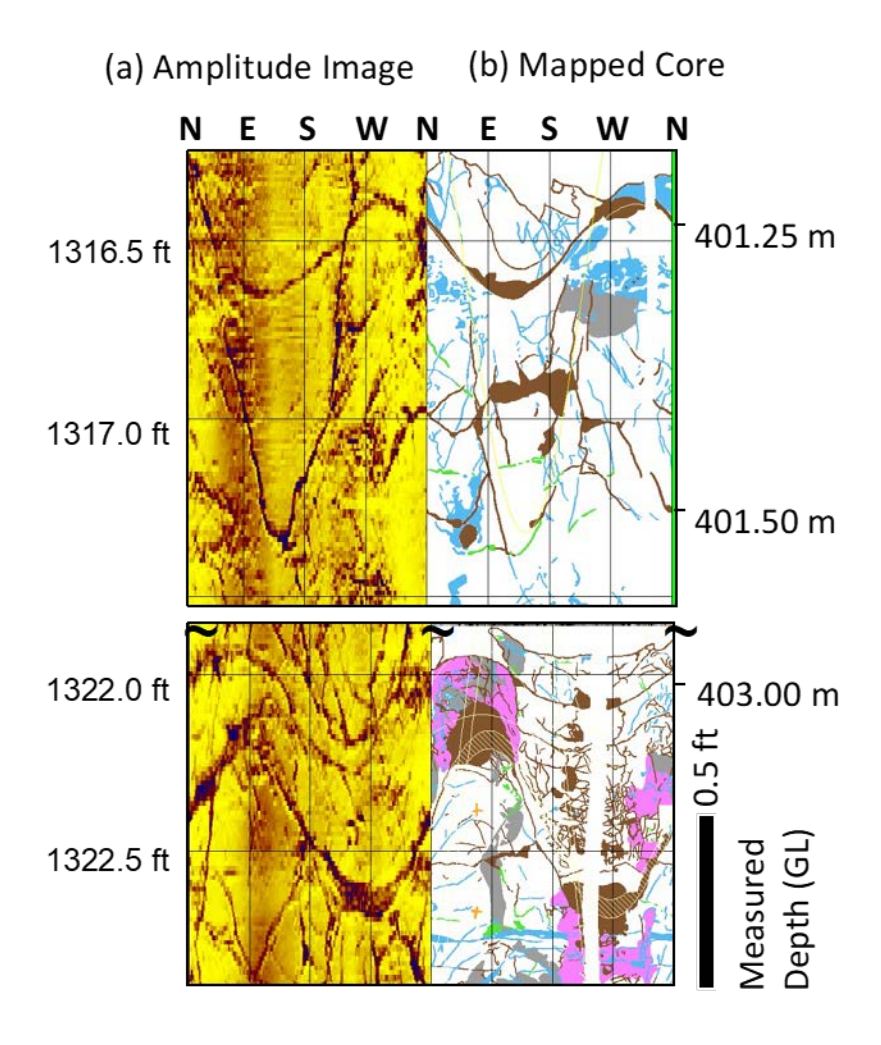


Figure 7: Fractures in BHTV and core. Legend in Figure 6.

3.2 Image Logging

Borehole Televiewer Logs (BHTV) from 314.8 m to 445.2 m (1032.7 ft to 1460.7 ft) measured depth were obtained in 2019 with a Robertson High Resolution Acoustic Televiewer (HRAT). The tool generates images of two-way travel time and amplitude of the returned pulse that provide a 360-degree view of the TGH wall with a nominal 5 mm pixel size. An advantage of this tool is the ability to manually adjust the amplitude of the initial pulse and the time gate to detect the return pulse in real-time during logging to maintain wall detection throughout the run.

The resulting images have been imported into WellCAD, where they are oriented relative to magnetic north by a three-component magnetometer and the deviation from vertical by a three-component accelerometer. The image log is then translated to a ground level (GL) datum and tested against the measured depth of the casing shoe. Maximum deviation from vertical over the logged interval is 2.3° at the base of the hole.

Roughness due to fractures intersecting the borehole wall scatter the acoustic pulse and thus appear as low amplitude and longer two-way travel time or missing signal. The azimuthally unwrapped image of the borehole surface then reveals planar structures that intersect and roughen the borehole wall as sine waves (Figures 5 and 6). The thickness of these structures depends on the true mechanical thickness (or aperture if open) of the feature, its angle of intersection with the TGH, and any erosion along the trace of the intersection with the TGH wall. The position, attitude, apparent aperture (better described as apparent thickness), and type of these features are then interpreted.

BHTV analysis typically takes 3-5 working days for interpretation and QA of 1000 ft (~300 m), followed by data analysis.

3.3 Mineralogy and Paragenetic History

After mapping, thin sections were made to characterize mineralogy, texture, alteration, and pore structure of the (1) host rock and (2) precipitants in fractures. For each thin section, powder x-ray diffractograms (XRD) of bulk mineralogy have been measured to further characterize the mineralogy. Additional measurements have been obtained for field samples representing the major formations in the vicinity of MB 76-31. Samples were powdered to less than 150 microns. Then, measurements of core have been obtained for 2° to 70° degrees two-theta in 0.01° increments with 1 second dwell times on a Bruker d8 using a copper K-Alpha x-ray source at 40 kV and 40 mA. Measurements of the reference samples have been obtained for 3° to 57° degrees two-theta in 0.04° increments with 0.5 second dwell times on a Rigaku Geigerflex using a copper x-ray source at 45 kV and 20 mA. Mineralogy is inferred from fitting the resulting peak distribution using TOPAS.

4. Results

4.1 Results of mapping and mineralogical analysis

4.1.1 Host Rock Mineralogy and Texture

The host rock is primarily comprised of Albite and Anorthite, Augite-Aegirine, Chlorite, microcrystalline and megacrystalline Quartz, Calcite, with smaller amounts of Chalcopyrite, Vermiculite, Epidote, and trace Graphite as deduced through XRD analysis. Composition percentages change throughout samples, though the majority have the same bulk composition (Figure 9b).

Thin sections reveal a fine-grained ground mass comprised with abundant clays. Plagioclase occurs as well-preserved phenocrysts with euhedral grain shape to several millimeters in length within a finer grained groundmass. Augite-Aegirine is mostly fine grained with some grains up to 0.5 mm; these grains show dissolution along cleavage with the new pores coated by microcrystalline quartz. Microcrystalline quartz also commonly fills secondary porosity from microfractures in phenocrysts and in dissolution preferentially developed along cleavage planes in phenocrysts.

Healed fractures are primarily comprised of Calcite, with some Chlorite and Quartz (Figure 9c). Quartz displays some undulose extinction and occurrence of subgrains. Chlorite and Vermiculite are also replacement minerals for some of the mafic phases as is Vermiculite and forms some of

the groundmass. If present, relative instability of cristobalite would be consistent with more recent hydrothermal activity.

Based on mapping by Tabor et al., (2003) and comparison to nearby outcrops, the core is interpreted to sample the volcanic rocks of the Chilliwack group comprised of partially metamorphosed volcanic rocks ranging from basaltic to andesitic. However, we note that due to faulting in this location and its similarity the Nooksack formation is an alternative interpretation. Both units show similar mineralogy (Figure 7a) to the host rock in the core (Figure 7b). Thus it is difficult to distinguish which unit the core represents without analysis of a more extensive interval.

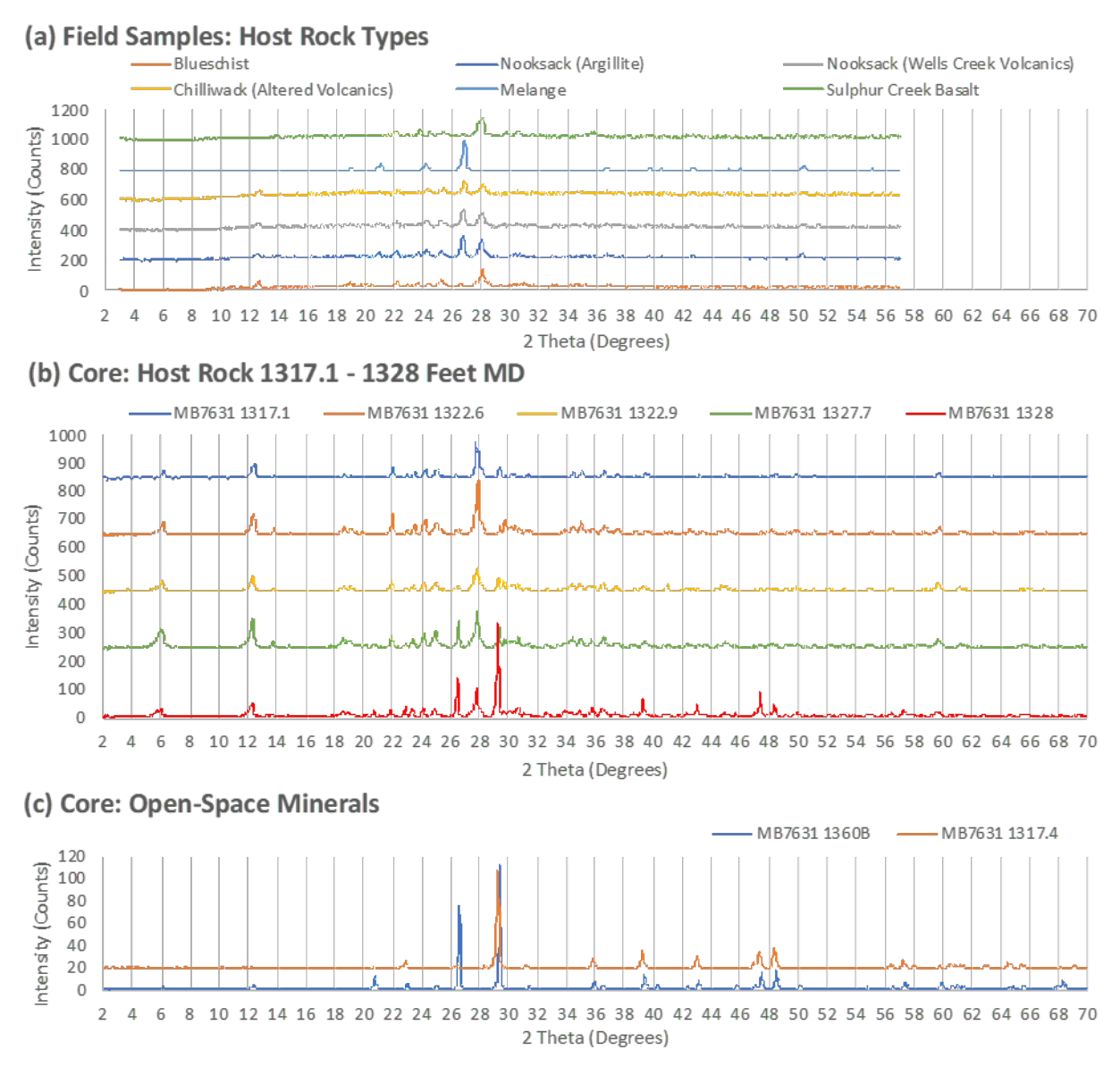


Figure 8: X-Ray spectra for (a) representative host rock samples, (b) host rock and (c) open-space minerals in core from MB76-31.

4.1.2 Fractures and Faults

The rock hosts four distinct fracture types (Figure 4, 6, 7): (a) well-developed fault zones several centimeters thick with (b) adjacent high fracture density within a few tens of centimeters of the fault, (c) microcracks up to a few millimeters long and less than about 0.1 mm thick, and (d) steeply dipping fractures that may extend for meters along the core.

Well-developed faults are characterized by healed breccia and fragmentation zones. The faults thus have irregularly boundaries. The faults have moderate dip and often contain slickensided slip surfaces with steep rakes indicating predominantly dip slip faulting. In fault zones, healing is largely complete with thicknesses of several centimeters. Diffractograms (Figure 8) and thin sections (Figure 8) reveal pore-filling minerals are mostly calcite with quartz along margins or sometimes calcite inter-grown with fibrous quartz or clumps of quartz grains. On some faults, chlorite forms foliated and slickensided coating. Chlorite is also present as a replacement and vein filling mineral throughout the host rock.

However, fractures adjacent to these faults are only partially healed (Figure 4). These fractures occur at two distinct length-scales and attitudes including fractures parallel (synthetic) or antithetic to the fault that span the entire core diameter and smaller fractures confined between them. The larger fractures show millimeter shear offsets and similar thickness. These fractures are at least partially healed, but often contain short segments of open space where the combination of slip and roughness produces larger aperture (Figure 4, Figure 9). Abutting the larger fractures are small splay fractures with (a) that intersect the older fracture at approximately 70° and (b) show primarily opening (no shearing) that is (c) opening up to 10% of their length. These fractures host some open porosity, but are more often coated or healed by calcite. The majority of the currently open porosity is in these incompletely healed fractures and pore spaces which are typically less than 1 cm long and 1 mm thick. Despite their abundance, macroscopic pores along fractures appear to be highly isolated (consistent with the apparently conductive temperature gradient measured in the well).

Steeply dipping fractures are discontinuously healed by calcite. Opening on these fractures exceeds indicators of shearing along the crack suggesting tensile failure. The cement is layered, and shows repeated dilation followed by calcite precipitation. Despite being nearly parallel to the borehole axis, they are well represented in core. These fracture both cut and are cut by faults indicating penecontemporaneous formation.

The host rock also exhibits variably developed clay alteration near faults (Figure 9). These zones contain abundant braided clay seams that offset primary feldspar grains and secondary veins. These zones also contain short, thick fractures with high aspect ratio as well as sigmoidal calcite veins and chlorite veins which may include internal cracks. All three features indicate semi-brittle ductile flow; since this flow is evident in altered host rock adjacent to a slickensided fault and deforms veins, it is determined to be tectonic although syn-deposition flow is common in volcaniclastics.

A critical result of the detailed core maps is that the majority of fractures throughout the map have lengths less than the core diameter. This is especially true in fragmentation and breccia zones associated with well-developed faults. In addition, the aperture of features is rough, irregular, and discontinuous due to partial healing. Fracture connectivity is high via small-length

fractures that bridge the interval between the larger fractures, but open pore space is discontinuous. Subsection headings should be capitalized on the first letter. Avoid using subsections deeper than subsubsections.

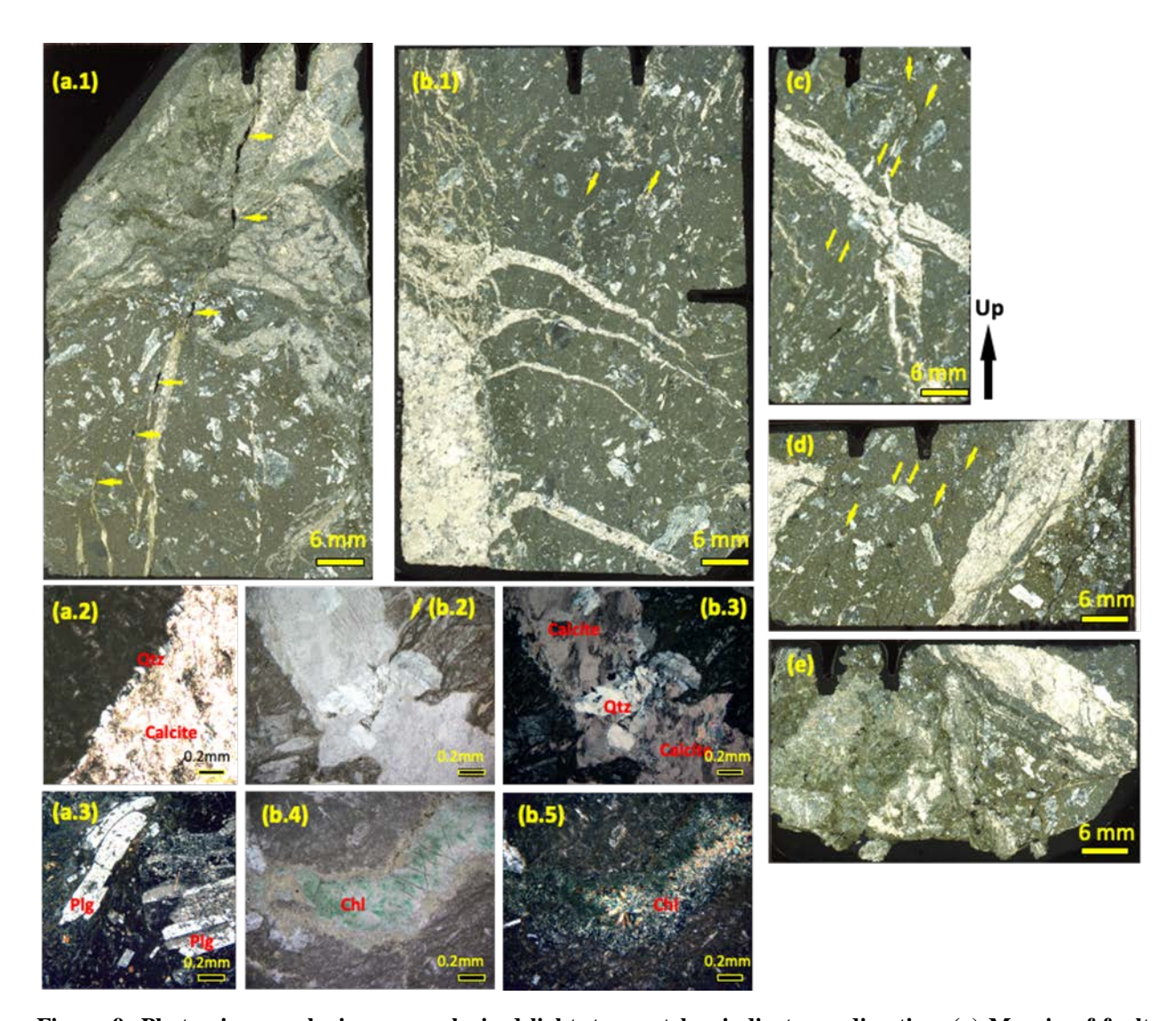


Figure 9: Photomicrographs in cross-polarized light, two notches indicate up direction. (a) Margin of fault zone at 403.13 m (1322.6 ft) MD; note the pores along a partially healed, near vertical fracture. (a.1) Massive calcite over microcrystalline quartz at the margin of a fracture. (a.2) Groundmass squeezed between two plagioclase grains. (b) Vein with network of microcracks at 404.68 m (1327.7 ft) MD; note the sigmoidal geometry of some veins associated with a network of microcracks healed by calcite and clay seams. (b.2 and b.3) show deformed quartz bridging a fracture otherwise healed by calcite. (b.4 and b5) show sharing and bending of a fracture filled by chlorite. (c) Fracture showing multiple cement layers in segmented fractures cut by clay seams at 404.50 (1317.1 ft) MD. (d) Layered vein from 401.54 m (1317.4 ft) MD with detailed images in plane polarized and cross polarized light. (e) Brecciated host rock from 404.77 m (1328 ft) MD showing grain cracking and layered cementation. All sections show discontinuous open fractures (black) also evident in core samples. Along the clay seams, the open space may be due to plucking during thin section preparation.

4.2 Fracture statistics from image logging

The BHTV log reveals fractures throughout the imaged interval (Figure 10) in a wide range of attitude (Figure 11). Notably, fracture density typically exceeds 4/m, except in the interval from 340 to 360 meters which has significantly lower density (despite good image quality). The fractures do not appear to group into distinct sets, although the features with the largest apparent aperture strike NE-SW and dip steeply northwest. Somewhat surprisingly for a near vertical well (which is biased toward sampling shallowly dipping structures), nearly vertical fractures are well-represented in this distribution. Some intervals also include progressively rotating fracture attitude (e.g., 360 to 368 m MD) which might result from the bias of the interpreter to pick fractures with attitude similar to earlier picks.

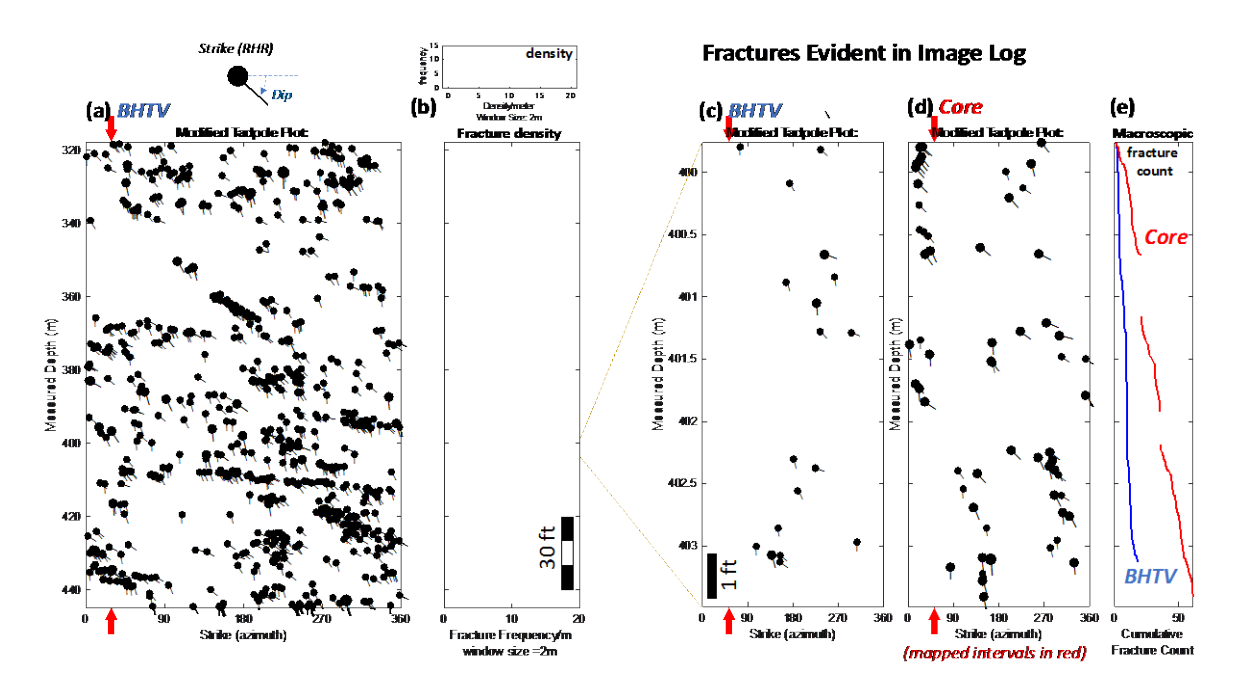


Figure 10: Tadpole plot showing the distribution of fracture attitude in TGH MB 76-31. Note that tadpole position indicates the strike azimuth with the dip azimuth to the east of strike according to the right-hand-rule. Dip is indicated by the steepness of the tail (see inset). Symbol size is proportional to apparent aperture or thickness of the feature in the image log or core. Red arrow indicates the anticipated strike of major faults mapped in vicinity of MB76-31 (Tabor et al., 2003; Forson et al., 2017). (a) Fractures interpreted in the BHTV throughout the logged interval and their associated (b) density per meter. Comparison of the results from BHTV and core are show in (c) and (d) respectively. (e) shows that the cumulative fracture counts form (c) and (d) is much larger for core than BHTV. Note that this is the count of macroscopic fractures that transect the entire core map and are well-represented by sinewayes.

4.3 Comparison of BHTV and Core Fracture Analysis

BHTV interpretation is more amenable to picking large fractures that fully traverse the TGH wall and that host open porosity or weak mineral filling that produces roughness at the fracture walls (Figure 7) (Table 1). This is actually pre-supposed by the process of fitting sine waves to fracture

traces to determine the strike and dip of fractures. Since small fractures and discontinuously healed fractures host the majority of macroscopic open porosity, both the image log and the standard workflow for its interpretation clearly under-estimate host rock porosity.

In the 3.8 m interval mapped by image log and core, 15 fractures spanning the full diameter of the borehole are interpreted from the BHTV image (Figure 10). Typical density is 4 to 6 fractures per meter. Whereas core reveals 61 fractures spanning the full diameter of the core; many additional fractures shorter than the borehole diameter are evident (which are sometimes misinterpreted as larger continuous fractures during BHTV image interpretation.

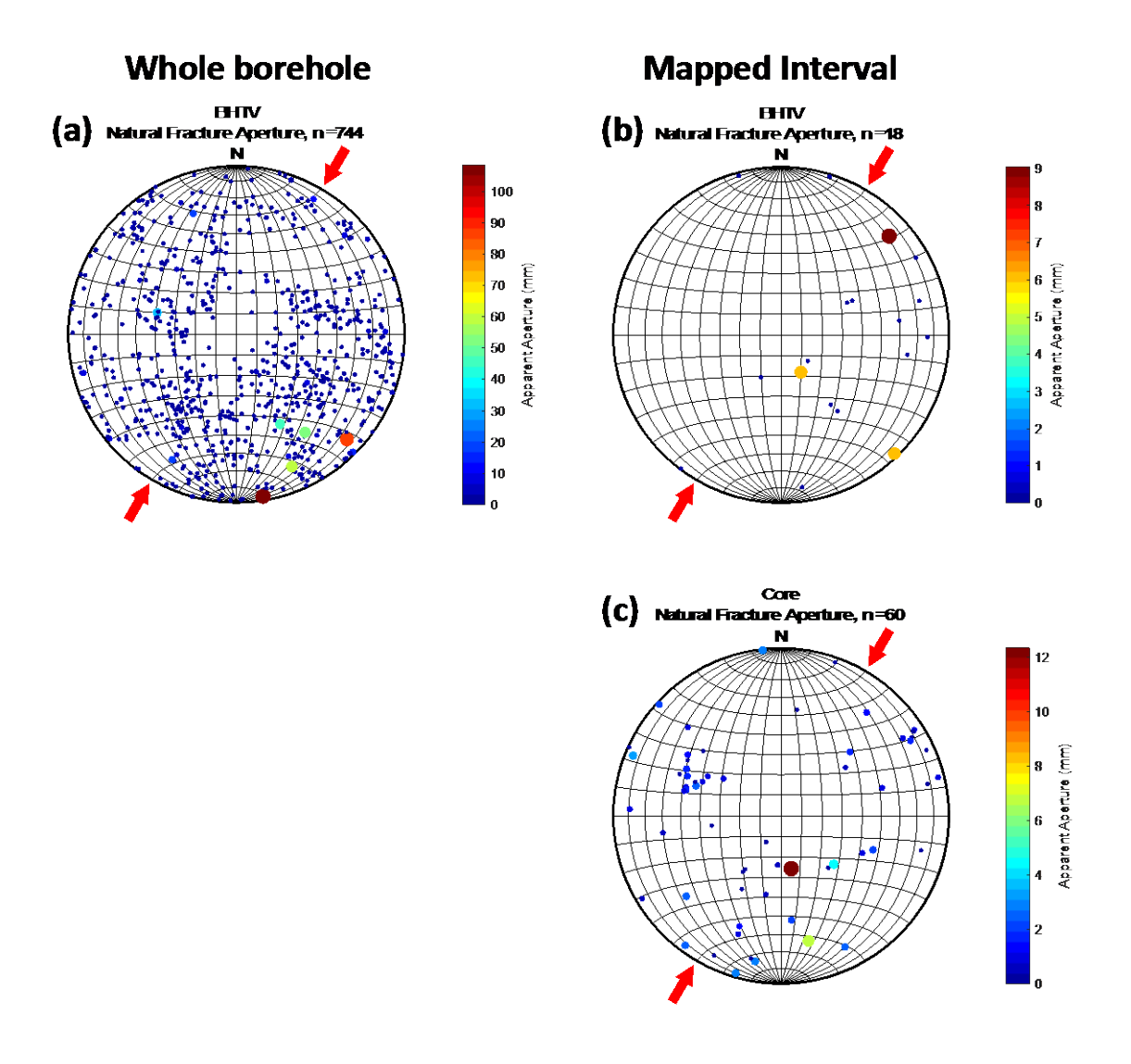


Figure 11: Stereograms of fracture attitude: (a) fractures interpreted from BHTV throughout the entire logged interval; fractures interpreted within the interval of mapped core in the (b) BHTV log and (c) core map.

In general, core maps document nearly four times as many fractures as BHTV (Figure 9e) including orientations not identified in core. Several factors appear to contribute to this discrepancy (Table 2). First, the resolution of the core map is higher (structures >5 mm long and 0.1 mm thick) than the BHTV (with a 5 mm pixel size likely to reveal roughness down to 1 mm). Second, highly cemented fractures are mostly not identified in the image log (Figure 6). Third, it is clear that in some cases, multiple independent fractures evident in core are interpreted as a single fracture in the image log; this mistake results in a mismatch in both the frequency and in the attitude of structures in the two analyses (Figures 10 and 11). However, the majority smaller fractures evident in the core whether open or healed were not identified in the image log. Subsection headings should be capitalized on the first letter.

4.3.1 Table 1: Interpretation by structure type

Feature	Image Log	Core and Map	
Open Fractures	Sine waves of low amplitude.	Open space not filled with precipitants or original rock. Segments core unless partially healed.	
Fractures healed by calcite	May be absent in amplitude image or as appear faint traces; traces may be discontinuous.	Fractures or inclusions filled with calcite or quartz; healed or partially healed.	
Fractures healed by chlorite	Sine waves of low amplitude; may be discontinuous but are evident.	Fractures or inclusions filled with chlorite; healed or partially healed.	
Breccia	Zones fully healed by calcite may be partially imaged or not evident. Partially healed breccias with open space appear as irregular low amplitude patches defining discontinuous sine waves.	Heavily altered and complex segments that are mostly healed. Larger portions of precipitants and open fractures are mapped within the more complex area.	
Handling fractures	Not present; occasionally faint amplitude trace where handling fracture is located on a weak geological feature.	Fragmented core or complete fractures mapped as open space. Orientation varies but are often either sub-horizontal or along natural structures evident in image Log.	
Boundary between lithologies	Not evident for these lithologies (although strong lithologic transitions commonly observed by other studies).	Sinusoidal (planar) to irregular trace consistent with syn-emplacement deformation. Edges may be blurred by associated alteration.	

4.3.2 Table 2: Sampling bias by technique

Feature	Image Log	Core and Map	Implication
Fracture	Interpreted fractures all exceed	Majority of fractures have	Under-estimate fracture
Length	the borehole diameter.	length less than core diameter:	porosity.
, and the second		Fragmentation, proto-breccia	Characterization of fault
		and breccia.	damage zones limited in image
			Log.
Fracture	Aperture is overestimated due	Aperture is rough, irregular,	Core shows a more tortuous
aperture	to: (1) Analysis fits constant	and discontinuous due to partial	potential flow path than implied
& healing	aperture to structure; (2)	healing.	by macroscopic fractures
	Aperture appears enhanced by	Associated aperture can be	mapped in image logs.
	erosion at borehole wall.	precise if calculated from pixel-	Both core and image log reveal
	Healed veins may not be	based image analysis.	pore discontinuity due to partial
	evident.		healing.
Connect	Connectivity is attributed to	Connectivity is high via small-	Image log under-estimates
-ivity	fractures greater than borehole	length fractures that abut larger	connectivity and porosity by
	diameter.	fractures.	small fractures.
Bias	Large, flat fractures defined by	Biased toward regions of low	Confirmation bias is an
	sinewaves.	fracture density or well-healed	important source of error in
	Small fractures mistakenly	fractures.	image log analysis.
	connected to define fractures	Borehole parallel veins are well	Small or vertical fractures are
	introduce erroneous attitudes	established and mapped.	not well represented in image
	and non-existent connectivity.		log analysis.
Complete	Continuous relative position	Missing core is associated with	Core and image logs likely to
-ness &	maintained.	large faults or open fractures.	miss data in same intervals.
Depth	Borehole wall rugosity yields	Introduces some positional	
control	pore image quality at large	uncertainty.	
	structures.		

5. Synthesis

5.1 Fractures at Mount Baker

The PFA model predicted high fracture density at MB76-31 from modeling of stress changes associated with faulting (Swyer et al., 2018) along lineaments mapped by Tabor et al. (2003) and evident in LiDAR (Forson et al., 2017). High fracture density is necessary to provide both storage of hydrothermal fluids and a connected network that can assist heat transfer through advection (Forson et al., 2017). In addition, the model relies on faulting to extend the network of percolating fractures to a heat source at depth.

Overall, the host rock has little matrix porosity owing to clays that squeeze around harder grains (e.g., Figure 9a.3) or precipitation of microcrystalline quartz, chlorite, or calcite. The image log and core analysis both indicate high fracture density and reveal abundant intersections. The fractures have clearly dilated the rock through a combination of effective tensile opening and dilation resulting from dilation accompanying shear on rough surfaces. In addition, well developed faults are also present with associated brecciation and slickensided slip surfaces. These fault zones are thoroughly healed by calcite, chlorite, and minor quartz. Porosity does occur in the fractures adjacent damage zone and in the steeply dipping fractures; however partial healing by calcite in both results in isolated macroscopic pores.

The relative isolation of pores is consistent with the measured conductive temperature gradient in the TGH (Cladouhos et al., 2020, Figure 2e).

5.2 Hydrothermal History of Rock and Fractures Transected by TGH MB76-31

With a maximum depth of approximately 440 m, TGH 76-31 is too shallow to penetrate the hypothesized geothermal resource. It is deep enough to possibly detect a hydrothermally altered, clay-rich caprock above such a resource. A caprock typically includes variation in alteration mineralogy reflecting increasing temperature with depth; temperature stability of minerals in the cap have significant overlap, so the emphasis is typically on the high temperature cutoff above which minerals should be absent (Wohletz and Heiken, 1992; Meunier and Velde, 2004; Heunges, 2010; Fulignati, 2020). At shallow depth and temperature, smectites dominate; smectite should be largely absent at temperatures over 160-210°C. Then as temperature increases, alteration progresses to mixed-layered smectite-illite (<150-220°C) and chloritesmectite (<160-250°C), then to illite and chlorite (220°-350°C), although some chlorites may form as low as 80°C); epidote may also form in the chlorite temperature range. These ranges should be treated with care as the kinetics of these transitions complexly depend on the initial mineral assemblage, chemical conditions such as pH, duration, and fluid chemistry and flow. The abundance of phyllosilicates reduces the frictional strength of the rock (expandable clays: 0.18-2.2, chlorite: 0.38, illite: 0.43, Lockner and Beeler, 2002), and thus reduces differential stress the rock can support. Alteration is expected to be most intense where upwelling hydrothermal flow is directed through faults. This combination of frictionally weak minerals and low differential stress in fault zones suppresses dilatant failure in preference to creep within faults (as discussed in Davatzes and Hickman, 2010a).

The current assemblage of authigenic minerals filling secondary porosity and replacing primary minerals is dominated by calcite plus chlorite plus vermiculite. Clay and chlorite alteration are especially well-developed in faults and the adjacent highly fractured damage zone. This rock deforms by a combination of dilatant brittle failure evident from calcite veins and calcite cemented breccia with ductile flow evident from shearing along clay seams, folding and rotation of veins, and impingement of clays between plagioclase grains. Ductile flow and healing by calcite precipitation could account for low porosity and relatively isolated pores that should act as a low permeability caprock.

Vermiculite implies lower temperature alteration consistent with measured temperatures in the TGH (Fulignati, 2020). Chlorite however implies higher authigenic temperatures. Since chlorite occurs in these relatively low modern temperatures, it is most likely that it is remnant from earlier greenschist metamorphism. Its presence in the faults can then be attributed to preferential incorporation due to relative weakness (static friction coefficient of ~0.38 for chlorite versus 0.85 for plagioclase or calcite, as summarized by Lockner and Beeler 2001).

Alternatively, ductile flow may be related to emplacement and diagenesis of hot volcanics and regional greenschist metamorphism accompanying convergence since Devonian deposition (Tabor et al., 2003). Such metamorphism is consistent with chlorite which replaces grains throughout the samples. However, clay seams cut and offset veins indicating more recent activity. Extensive networks of microcracks intermixed with alteration also suggest penecontemporaneous activity. At these shallow depths it may also be expected that weathering

facilitated by groundwater flow could account for the formation of clays. However, preservation of chalcopyrite in the rock suggests the waters moving through this rock are not from the surface.

To distinguish the presence of a caprock from these other processes will require additional core at greater depth to determine if higher temperature minerals replace clays. Such deepening would also provide an additional test of the potential resource temperature. A 3.3 km TGH is necessary at the current gradient of $\sim 60^{\circ}$ C/km.

5.3 Comparison of structural analysis by core and image log

Core reveals approximately four times as many fractures spanning the full diameter of the TGH as the BHTV similar to results by Genter et al. (1997) in granite. Although some fractures are picked in both logs with similar attitude, several fractures in picked in the image log do not match fractures evident in core. This appears to result from mis-interpreting complex fractures or multiple smaller fractures as a single, throughgoing structure. Picks of fracture attitude appear to also depend on prior experience in the log. Thus image log interpretation may be more prone to confirmation bias leading to a narrower range of picked fracture attitudes and progressive evolution of attitude with picking depth as the analyst works through the image. This is promoted by the workflow that requires fitting a sine wave to record both the presence of the fracture and obtain adequate information to calculate attitude. This bias can be mitigated by using quality rankings to separate fracture picks of high quality useful for calculating attitude from lower quality picks (typically with incomplete sine waves) useful only for computing fracture density (Davatzes and Hickman, 2010b).

BHTV is an effective and practical means of assessing fracture populations, but is prone to several biases due to complex fracture geometry, rock-dependent sampling, and poor sampling of fractures shorter than the borehole diameter, healed and partially healed fractures critical to interning tectonic history and potential for fracture porosity and which may influence potential for stimulation; detailed mapping of core reveals these biases, but requires extensive time but provides a benchmark to calibrate the representation obtained from BHTV logs. We note that although in this case no borehole wall failure is observed in the BHTV logs to constrain the stress state, core would not be capable of effectively capturing these features.

It is also clear that small fractures shorter than the borehole diameter are critical to the porosity structure and potential connectivity in this core. These structures are wholly overlooked by the current workflow for image log analysis.

5.4 Future work and recommendations

Following Genter et al. (1997), as more core is mapped it will be useful to characterize the fracture spacing distribution derived from core and image log. This will provide a basis for benchmarking the image log. Similar work could be done for the distribution of fracture lengths in the core and for pore shape, size, and position and filling (open, chlorite, vermiculite, silica, calcite, combinations).

Next steps including continued core mapping and associated characterization of the mineralogy and pore structure to test for variation through depth or with rock type. We will also consider alternative workflows for analyzing fracture distribution, such as analyzing the pixels of the digitized core maps or a similar mapping approach applied to the image log. Although it does not

address the problem of characterizing fracture attitude, fracture frequency and aperture distribution may be better estimated by analyzing the pixel density of interpreted structure maps.

6. Conclusion

Core from MB76-31 contains abundant faults and associated high fracture density. Fractures are well connected and document extensive dilation in the rock, but due to extensive healing, open pore are currently isolated. These faults are spatially associated with phyllosilicates that assist ductile deformation coeval with these dilatant fractures and may indicate a developing caprock. Inferred low permeability is consistent with the measured conductive temperature gradient more than twice the regional average. Testing the caprock hypotheses requires more vertically extensive coring and mapping to establish trends in temperature sensitive mineral phases.

Analysis of core reveals approximately four times as many borehole-transecting fractures as interpreted from the BHTV log. The majority of fractures are confined within core, and these smaller fractures tend to host the open pore space – these fractures are not identified by image log analysis. In addition, the resulting complexity in fracture geometry causes uncertainty in the attitude of fractures interpreted from image logs producing greater scatter in attitude than in the core analysis.

Acknowledgement

This research was generously funded by the U.S. Department of Energy Geothermal Technologies Office, grant #DE0006728 awarded to the Washington State Department of Natural Resources. Support was also provided by the Washington State Department of Natural Resources, Washington Geological Survey. Alexandra Davatzes provided feedback on thin section interpretation. Justin Morris supported XRD measurement and analysis at Temple University. Peter Stelling provided an introduction to the geological setting, access to both representative outcrops of key formations and to XRD facilities at Western Washington University.

REFERENCES

- Blackwell, D.D., Steele, J.L., Kelley, S., and Korosec, M.A. (1990) Heat flow in the state of Washington and thermal conditions in the Cascade Range. Journal of Geophysical Research, v. 78, p.
- Blackwell, D. D., 2010, Updated and combined Regional Heat Flow and Western Geothermal Area databases; Washington State: Southern Methodist University, 1 Excel spreadsheet. [accessed Sept. 25, 2010 at http://smu.edu/geothermal/georesou/washingt.htm]
- Boschmann, D. E.; Czajkowski, J. L.; Bowman, J. D. (2014) Geothermal favorability model of Washington State: Washington Division of Geology and Earth Resources Open File Report 2014-02, 1 plate, scale 1:900,000, 26 p. http://www.dnr.wa.gov/publications/ger_ofr2014-02_geothermal_favorability.pdf

- Cladouhos, T.T., A. Steely, N.C. Davatzes (2021) Washington State Play-Fairway Analysis: Preliminary TCH Drilling Results. Geothermal Resource Council 2020 Virtual Annual Meeting & Expo, abstract.
- Crider, J. G., Frank, D., Malone, S. D., Poland, M. P., Werner, C., & Caplan-Auerbach, J. (2011). Magma at depth: a retrospective analysis of the 1975 unrest at Mount Baker, Washington, USA. Bulletin of Volcanology, 73(2), 175-189. https://doi.org/10.1029/JB095iB12p19495
- Davatzes, N.C., and Hickman, S.H. (2010a). Stress, fracture, and fluid-flow analysis using acoustic and electrical image logs in hot fractured granites of the Coso geothermal field, California, U.S.A., in M. Poppelreiter, C. Garcia-Carballido, and M. Kraaijveld, eds., Dipmeter and borehole image log technology: AAPG Memoir 92, Ch 24., p. 1 35.
- Davatzes, N., Hickman, S. (2010b). The Feedback Between Stress, Faulting, and Fluid Flow: Lessons from the Coso Geothermal Field, CA, USA. Proceedings World Geothermal Congress 2010
- DeAngelo, J.; Shervais, J. W.; Glen, J. M.; Nielson, D.; Garg, S.; Dobson, P.; Gasperikova, E.; Sonnenthal, E.; Visser, C.; Liberty, L. M.; Siler, D.; Evans, J. P.; Santellanes, S., 2016, GIS methodology for geothermal play fairway analysis—example from the Snake River Plain Volcanic Province: Stanford Geothermal Workshop, 10 p.
- Dragovich, J.D., Logan, R.L., Schasse, H.W., Walsh, T.J., Lingley, W.S.J., Norman, D.K., Gerstel, W.J., Lapen T.J., Schuster, J.E., and Meyers, K.D., 2002, Geologic map of Washington—northwest quadrant: Washington Division of Geology and Earth Resources, Geologic Map GM–50, 1:250,000, 3 sheets, booklet 72 p.
- Fetterman, J.D. and Davatzes, N.C. (2011) Evolution of Fracture Porosity in the Newberry Volcano Geothermal System, Oregon, USA: Feedback between deformation and alteration. Geothermal Resources Council Annual Meeting, San Diego, CA. 7 p.
- Forson, C., Czajkowski, J. L., Norman, D. K., Swyer, M. W., Cladouhos, T. T., & Davatzes, N. (2016). Summary of Phase 1 and Plans for Phase 2 of the Washington State Geothermal Play- Fairway Analysis. Geothermal Resources Council Transactions, 40, 541-550.
- Forson, C., Steely, A.N., Cladouhos, T., Swyer, M., Davatzes, N., Anderson, M., Ritzinger, B., and Stelling, P. (2017). Geothermal Play-Fairway Analysis of Washington State Prospects: Phase 2 Report and Phase 3 Proposal. Unpublished, 1-52. https://gdr.openei.org/submissions/994
- Forson, C., N.W. Swyer, G.M. Schmalzle, J.L. Czajkowski, T.T. Cladouhos, N.C. Davatzes, Nand R.A. Cole (2015). Geothermal Play-Fairway Analysis of Washington State Prospects. Geothermal Resources Council Transactions, 39, 701-710.
- Fulignati, P. (2020) Review: Clay Minerals in Hydrothermal Systems. Minerals, v.10, 19 p. doi:10.3390/min10100919
- Genter, A., C. Castaing, C. Dezayes, H. Tenzer, H. Traineau, T. Villemin, (1997) Comparative analysis of direct (core) and indirect (borehole imaging tools) collection of fracture data in the Hot Dry Rock Soultz reservoir (France). Journal of Geophysical Research, v 103, p. 15419-15431.

- Hodge, B.E., and J.G. Crider. 2010. Investigating mechanisms of edifice deflation, 1981-2007, at Mount Baker volcano, Washington, United States. Journal of Geophysical Research, v. 115, doi:10.1029/2009JB006730.
- Huenges, E. (editor) (2010) Geothermal Energy Systems; Exploration, Development, Utilization. Wiley Press, 463 p. DOI:10.1002/9783527630479
- Hildreth, W., J. Fierstein, & M. Lanphere (2003). Eruptive history and geochronology of the Mount Baker volcanic field, Washington. Geological Society of America Bulletin, 115(6), 729-764.
- Lockner, D.A. and N.M. Beeler (2002), Rock failure and earthquakes. International Handbook of Earthquake and Engineering seismology in International Geophysics Series, edited by: Lee, W.H.K., H. Kanamori, P.C. Jennings, and C. Kisslinger. Academic Press, NY. v. 81A, p. 505-537.
- Meunier A., Velde B. (2004) Dynamics of the Smectite-to-Illite Transformation. In: Illite. Springer, Berlin, Heidelberg. Springer, 300 p. https://doi-org.libproxy.temple.edu/10.1007/978-3-662-07850-1_4
- Norman, D.K., C. Forson, J.L. Czajkowski, M.W. Swyer, T.T. Cladouos, G.M. Schmalzle, and N. Davatzes. 2015, Geothermal Play-Fairway Analysis of Washington State Prospects: Phase 1 Technical Report. 101 p.
- Saaty, T.L., 2008, Decision making with the analytical hierarchy process. International Journal of Service Sciences, v. 1, no. 1, p. 83-98.
- Spake, D., Steely, A.N., Cladouhos, T.T., Swyer, M.W., Forson, C, Davatzes, N.C. (2019) Geothermal Exploration North of Mount St. Helens: Washington State Play-Fairway Project, Workshop on Geothermal Reservoir Engineering 44, 19 p.
- Spake, Drew. (2019) Summary Report of Phase 3 Exploratory Drilling for the Geothermal Play Fairway Analysis of Washington State Prospects.
- Stowe, B., Davatzes, N., Spake, D., Cladouhous, T.T., Steely, A. (2020) Combined Structural Analysis of Core and Image Log of Borehole MB76-31 East of Mount Baker, Washington State. Geothermal Resource Council 2020 Virtual Annual Meeting & Expo, abstract.
- Swyer, M.W., T.T. Cladouhos, C. Forson, A.N. Steely, N.C. Davatzes (2018) Simulating Local Sources of Crustal Deformation for Washington State Geothermal Prospects using Geomechanical Models, ARMA,52nd US Rock Mechanics/Geomechanics Symposium and 2nd DFNE Conference 18–464, Seattle, WA, June 17-22, 2018. 9
- Tabor, R. W., & Geological Survey (US), (2003). Geologic Map of the Mount Baker 30 by 60 Minute Quadrangle, Washington. US Department of the Interior, US Geological Survey.
- Tabor, R.W., R.A. Haugerud, W. Hildreth, and E.H. Brown. 2003. Geologic Map of the Mount Baker 30- by 60-Minute Quadrangle, Washington. Prepared in cooperation with the Washington State Department of Natural Resources, Division of Geology and Earth Resources. Pamphlet to accompany Geologic Investigations Series I-2660. U.S. Department of the Interior. U.S. Geological Survey.

- Witter, J.B., D. Fournier, W.D. Schermerhorn, and P. Stelling (2017) Geophysical Inversion Modeling of Ground Magnetic Data at Baker Hot Springs, Washington State, USA. GRC Transactions, v. 41, 15 p.
- Wohletz, K. and Heiken, G. (1992) Volcanology and Geothermal Energy. University of California Press, Berkeley, CA. http://ark.cdlib.org/ark:/13030/ft6v19p151. 498 p.